Field-driven ultrafast sub-ns programming in W\Al_2O_3\Ti\CuTe-based 1T1R CBRAM system

L. Goux[1]*, K. Sankaran[1,2], G. Kar[1], N. Jossart[1], K. Opsomer[1], R. Degraeve[1], G. Pourtois[1], G.-M. Rignanese[2], C. Detavernier[3], S. Clima[1], Y.-Y. Chen[1,4], A. Fantini[1], B. Govoreanu[1], D.J. Wouters[1,4], M. Jurczak[1], L. Altimime[1], J.A. Kittl[1]

[1] imec, Kapeldreef 75, B-3001 Leuven, Belgium (*e-mail: gouxl@imec.be, phone: +32-16-28.87.47)
[2] UCL and ETSF, B-1348 Louvain-la-Neuve; [3] University of Gent, 9000 Gent; [4] KUL, Leuven, Belgium

Abstract – *We optimize a 90nm-wide CuTe-based 1T1R CBRAM cell for highly controlled and ultrafast programming by engineering Al_2O_3 electrolyte and Ti buffer layers of appropriate density and thickness resp. By means of electrical and ab initio modeling, we demonstrate that switching is mainly controlled by field-driven motion of Cu^+ species. Sub-ns programming is allowed by strong ionic-hopping barrier reduction over short insulating gap. Complete picture of conductance and switching phenomenology is shown in the entire operation range.*

Introduction – Conductive-Bridging RAM (CBRAM) is based on the electrochemical formation/disruption of a metal (mostly Cu or Ag) nanofilament through an insulating electrolyte induced by electrical pulses. Due to scaling potential and fast switching speed, CBRAM is considered as a serious candidate for future memory replacement [1]. This promise depends on the detailed microscopic switching mechanisms, which are however still under debate. In this paper we optimize a 90nm W\$Al_2O_3$\Ti\$Cu_{0.6}Te_{0.4}$-based CBRAM cell stacked on top of select transistor (1T1R scheme), and we address the switching and filament characteristics both from electrical and ab initio viewpoints.

W\electrolyte\buffer\Cu_xTe stack optimization – We selected the $Cu_{0.6}Te_{0.4}$ composition due to optimum switching control and performances [2]. Different insulators were tested as electrolytes. Atomic-Layer-Deposited (ALD) amorphous Al_2O_3 layers (a-Al_2O_3) showed best functionality (**Fig.1a-c**). Denser materials like thermally grown SiO_2 showed difficult programming of Low-Resistive State (LRS), which we attribute to the mechanically impeded growth of the Cu filament through a compact medium (**Fig.1d**). All screened materials showed similar relation between forming efficiency and porosity. This effect may be similar to the reported limited breakdown-induced epitaxy of Si through SiO_2 gate dielectrics [3]. Note that different deposition techniques of SiO_2 allowed effective CBRAM operation [4].

Due to in-diffusion processes of Cu and Te species through the Al_2O_3 layer during integration thermal budget (**Fig.2a**), we inserted a Ti layer at the interface. Thick Ti layers (6nm) completely suppressed the in-diffusion processes, which resulted in degraded CBRAM functionality. An optimum thickness of 3nm turned the *Cu-barrier* role of the Ti-layer into *Cu-buffer* role, allowing controlled Cu injection into Al_2O_3, and which resulted in both excellent switching and thermal stability. **Fig.3** shows the integrated optimized stack onto 90nm-wide W plug in a 1T1R configuration, and **Fig.4** shows the stack chemical integrity after integration together with the excellent switching control and cycling.

Switching phenomenology and state conductance – In agreement with SIMS results, ab initio calculation showed similar diffusivity of Te and Cu in a-Al_2O_3 medium (**Fig.5a**). However, in the situation of filament forming (potential decrease in **Fig.5b**), formation energy of Cu^{n+} species in a-Al_2O_3 is clearly favored over Te^{n+} species. Moreover, *Cu^{1+} species are the most likely generated cations* in the range between ~0.5V (onset of exothermic reaction) and 2.5-3V above which Cu^{2+} species may also be generated (**Fig.5b**). On the other hand, the bias required to generate a Cu filament (or LRS state) scales with the a-Al_2O_3 film thickness (**Fig.6a**), which would support that set switching *is limited by the field-driven transport* of generated Cu^{1+} species. In agreement, the set voltage V_{set} decreases if the filament is generated after partial filament erase (**Fig.6b**). Partial erase is the programming of intermediate High-Resistance State (HRS) due to the modulation of the filament dissolution, i.e. tuning of the gap δ between the filament tip and the cathode, which is controlled by the stop voltage V_{stop} during reset voltage ramp. Assuming same critical set field as for fully erased cells, δ may be estimated from cell resistance R_{cell} (**Fig.6c**). Based on this relation, **Fig.7** shows the switching and filament characteristics in the whole operation range. The cell may be operated within very-high resistance range using low transistor-controlled set current I_{set}<1μA, inducing partial filament growth and large δ, which in turn controls large reset voltage V_{reset}~1V (**Fig.7a**). State conductance (G) showed significant thermal activation, and may be dominated by hopping processes, as extrinsic defect states close to Fermi level were evidenced previously in the ALD-Al_2O_3 layer [5] (see also **Fig.8a**). CBRAM multilevel cell (MLC) operation is achieved with greater control within intermediate resistance range (**Fig.7b**). Various LRS states are modulated by I_{set} variation in the range 5-100μA. For I_{set}~5μA, short δ is formed and excellent control of R_{LRS}~100kΩ is obtained. Interestingly, ab initio density-of-states (DOS) calculations in a-Al_2O_3 showed the onset of band-like conduction regime as from a concentration of ~10^{21} Cu atoms/cm^3 (**Fig.8b**), suggesting possible electronic wave-function overlaps for δ<1nm. In this range R_{cell} may thus show weaker δ dependence (see **Fig.6c**), which together with the abrupt local-field decrease associated with this conduction regime change may account for excellent R_{LRS} control. On the other hand, for R_{LRS}~10kΩ, achieved using I_{set}~100μA, high-resolution voltage ramps revealed discrete jumps between fixed conductance slopes in agreement with quantized conduction in a point-contact configuration [6], which is consistent with the weak temperature dependence of G in this range (**Fig.7b**). Finally, larger I_{set}>300μA programs filaments in the range R_{LRS}<2kΩ, which results in fuse-blow type of reset. In that case, both the filament-temperature extraction using temperature-coefficient of G and calculation using realistic thermal conductance for Cu nanowires [7] confirmed thermal-dominated reset switching (**Fig.7c**).

Fig.9a shows a summary picture of the R_{cell}-dependence of V_{set} and V_{reset}. Note that V_{reset} shows a decrease with the increase of R_{cell} up to ~500kΩ, which corresponds to δ~0.8-1nm, and a V_{reset} upturn is observed above. This may again be related to possible abrupt conduction decrease (see **Fig.6c**), associated with temperature decrease and enhanced field-driven reset. This resistance range R_{cell}~500kΩ, showing lowest switching voltages, also exhibits weaker state stability (**Fig.9b**). In the larger R_{cell} field-driven range the reset field is similar to set field (symmetric traces in **Fig.9a**).

Voltage-time interplay – Reproducible and gradual state programming of the 1T1R cells was obtained using sequences of square pulses of rising amplitudes (**Fig. 10**). In the low-power operation range with best retention trade-off, pulse programming showed an exponential relation between switching time and voltage (**Fig. 11a**), which we could model using Mott-Gurney [8] field-induced barrier lowering allowing hopping of Cu^+ species. Excellent match was obtained using ab initio diffusion results and estimated δ parameter. The obtained hopping distance Δz~0.3nm could correspond to the spacing between oxygen sites in the a-Al_2O_3 matrix. Ultrafast <1nsec switching is obtained at >3V due to drastic barrier lowering combined with large effect of Δδ on R_{cell}.

Conclusion – We show the critical effect of electrolyte layer density on CBRAM functionality. By tuning of a 3nm-thick Ti Cu-buffer layer we integrate a thermally stable 90nm W\$Al_2O_3$\Ti\$Cu_{0.6}Te_{0.4}$ CBRAM cell showing excellent switching control. We show novel insights into filament-gap-dependent state conductance and switching mechanism, demonstrating also that low-power switching is limited by the field-driven hopping of Cu^+ species through Al_2O_3, in close agreement with ab initio simulation.

Acknowledgments – We acknowledge A. Franquet and O. Richard for physical characterization support.

References – [1] R. Waser et al., Advanced Materials 21 (2009) 2632; [2] L. Goux et al., IMW (2011); [3] C.H. Tung et al., IEEE Elect. Dev. Lett. 23 (2002) 526; [4] C. Schindler et al., Appl. Phys. Lett. 94 (2009) 072109; [5] K. Sankaran et al., Appl. Phys. Lett. 97 (2010) 212906; [6] R. Degraeve et al., IEDM (2010); [7] X. Lu, J. Appl. Phys. 105 (2009) 094301; [8] N. F. Mott et al., Electronic Processes in Ionic Crystals, Oxford (1948)

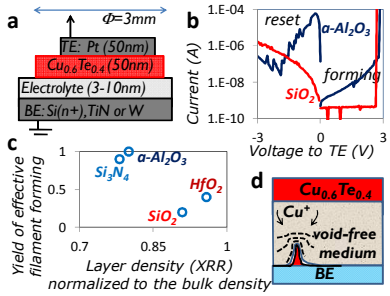

Fig.1: (a) test vehicle for stack optimization; (b) typical effective (ineffective) filament forming for ALD a-Al_2O_3 (thermal SiO_2) resp.; (c) forming efficiency versus layer density; (d) schematic showing impeded filament growth through compact (void-free) electrolyte materials

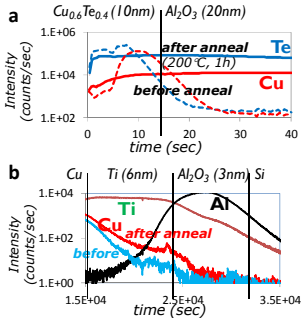

Fig.2: (a) SIMS profiles showing strong diffusion of Cu and Te into Al_2O_3 after anneal; (b) TOF-SIMS profiles showing effective *Cu-barrier* role of 6nm inserted Ti

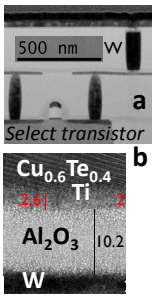

Fig.3: XTEM image of the 1T1R CBRAM cell (a), and close-up of the stack (b)

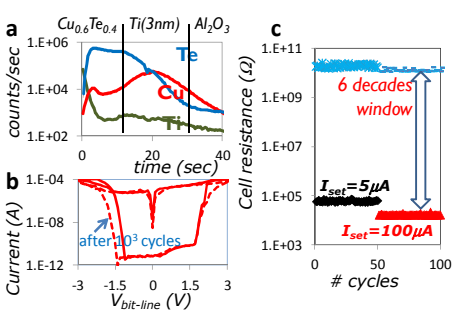

Fig.4: (a) SIMS profiles after integration thermal budget (200°C), showing effective *Cu-buffer* role of 3nm Ti layer; (b) I-V switching traces obtained for this optimum 1T1R cell, showing excellent control and cycling stability (c)

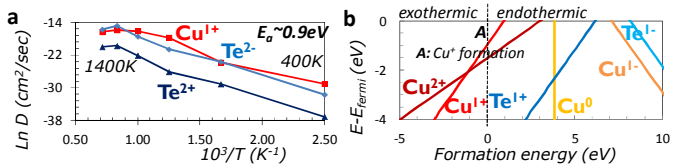

Fig.5: (a) ab initio diffusion calculations in a-Al_2O_3 medium, confirming that the elemental diffusion of Te is as pronounced as for Cu species; (b) ab initio formation energy calculations suggesting however preferential injection of Cu^{1+} cations over Te^{n+} and other Cu^{n+} species during forming (for moderate $V_{forming}$<3V), while too low voltages lead to endothermic cation formation (A)

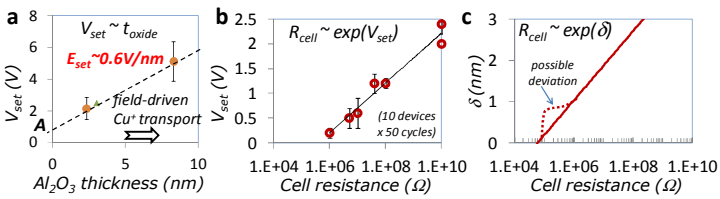

Fig.6: (a) Al_2O_3-thickness dependent V_{set} obtained after complete filament erase, suggesting field-driven filament formation; (b) cell-resistance dependent V_{set} obtained after partial filament erase (partial erase is controlled by V_{stop} during reset); (c) gap (δ) estimation derived from field-driven V_{set} data

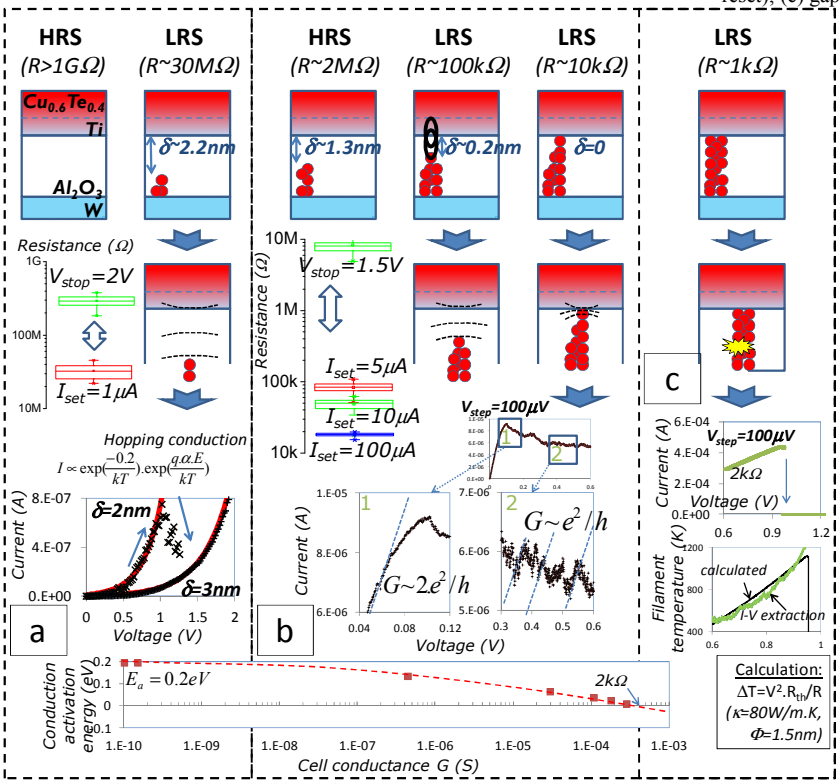

Fig.7: overview of the switching phenomenology depending on the operation range: (a) reversible high-resistance LRS programming (partial forming using I_{set}<1μA), whereby conductance is thermally activated and controlled by large δ; (b) reversible and highly controlled MLC programming to LRS states showing short δ or point-contact conductance (evidenced by high-resolution voltage ramp showing abrupt switch to discrete quantized conductance values); (c) metallic-filament programming, whereby abrupt fuse-blow-like reset switching is observed during high-resolution ramp, and whereby filament temperature modeling confirms the thermal-dominated reset (which alters the switching reversibility)

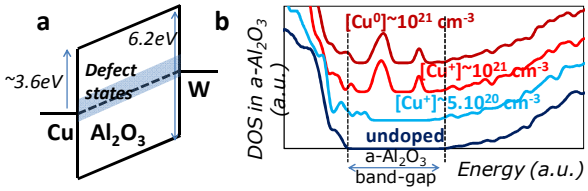

Fig.8: (a) band-diagram of the CBRAM structure during set operation, showing extrinsic defect levels close to Fermi level and presumably involved in HRS conduction; (b) ab initio DOS (GGA) calculation for a-Al_2O_3 doped with different densities of [Cu^+] or [Cu] species, showing onset of a band-like conduction regime as from ~10^{21} atoms/cm³ (1 atom/nm), consistent with short-δ LRS programming control

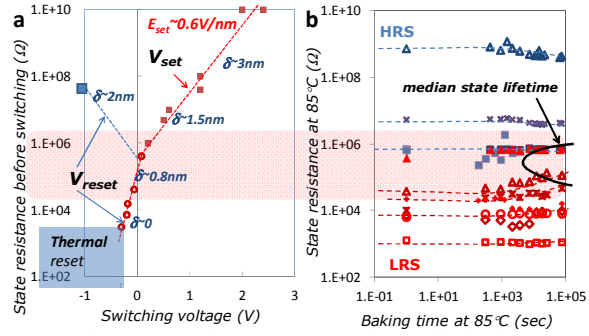

Fig.9: (a) different switching regimes: field-controlled set/reset for large δ, change of reset slope for short δ due to field confinement, and thermal-reset regime for metallic filament; (b) isothermal retention tests showing weaker stability in the resistance range corresponding to lowest switching voltages

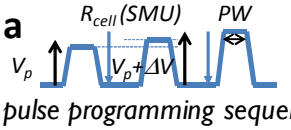

Fig.10: (a) pulse-programming sequence using fixed width and rising amplitude; (b) reproducible reset programming achieved for V_{pulse}<3V and PW=100nsec

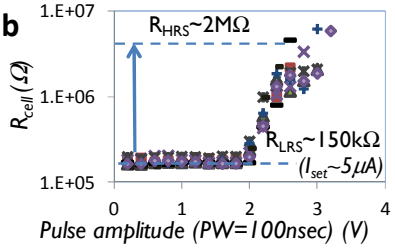

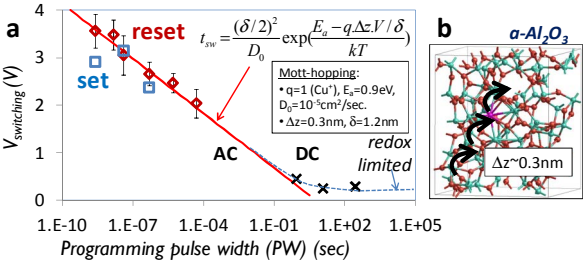

Fig.11: (a) PW-dependent reset and set pulse amplitudes, showing ultrafast switching within <1nsec for V_{pulse}<4V, and excellent match with Mott-hopping process of Cu^+ species (using parameters obtained by ab initio); (b) extracted hopping distance Δz is similar to spacing between O sites in ab initio generated a-Al_2O_3 model